AIAA JOURNAL
Vol. 30, No. 12, December 1992

Coupled Euler/Boundary-Layer Method for Nonequilibrium, Chemically Reacting Hypersonic Flows

S. Wüthrich* and M. L. Sawley†
Ecole Polytechnique Fédérale de Lausanne, Lausanne, Switzerland

A coupled Euler/boundary-layer method to calculate hypersonic flows in chemical nonequilibrium is described. Air chemistry is modeled by five species and a chemical scheme of 17 reactions. The coupled Euler/boundary-layer method consists of the successive solution of two sets of equations of increasing order in $Re^{-1/2}$, where Re is the Reynolds number. It is shown that, with the inclusion of second-order terms, a good matching of the calculated profiles at the interface between the inviscid and viscous regions can be obtained for both the chemical and thermodynamical properties. In addition, it is demonstrated that second-order effects play a major role in determining the surface coefficients for high Mach number flows. For hypersonic flow over a sphere, excellent agreement is shown between the calculated values of the surface coefficients and those determined from experiments.

Introduction

FOR re-entry flows at sufficiently high altitude and Mach number, the air in the region behind the bow shock is in chemical nonequilibrium. The numerical simulation of even steady, laminar flow is very complex due to the different chemical and flow time scales and to the large number of variables and partial differential equations required to describe the chemical and thermodynamical quantities. Past experiences have shown that simple physical models, which assume the flow to be either nonreactive or in chemical equilibrium, can lead to unrealistic predictions.[1] The use of the full Navier-Stokes equations for nonequilibrium flow simulations is, however, at the limit of current capabilities in terms of numerical algorithms, memory requirement, and computational time. One simplifying approach that has been adopted is to decouple the solution of the chemistry problem from the flow dynamics.[2] Alternatively, many studies have been undertaken that employ an approximate form of the Navier-Stokes equations that neglects certain viscous terms, such as viscous shock layer (VSL) or parabolized Navier-Stokes (PNS) methods. The coupled Euler/boundary-layer method described in the present paper can be viewed in this vein; it provides an efficient, accurate, and computationally inexpensive method that can account for the realistic modeling of nonequilibrium chemical effects.

Coupled methods are based on asymptotic matching theory, as described by Van Dyke.[3] For large Reynolds number Re, the viscous effects are limited to a thin region near the body surface described by the classical Prandtl boundary-layer equations. These equations have been used extensively for the analysis of viscous flow, due to both their simplicity and their parabolic nature. It can be shown[4] that these equations consist of the first terms of an asymptotic expansion of the Navier-Stokes equations near the wall in terms of the small parameter $Re^{-1/2}$. A similar expansion can be made for the flow region where viscous effects are small. This leads to two separate sets of equations: one valid in an inner (viscous) region (the boundary-layer equations) and another set of equations valid in the outer (inviscid) region (the Euler equations). A matching condition between the outer and the inner expansion has been proposed by Lagerstrom.[5] To second order in $Re^{-1/2}$, additional terms are present and new boundary conditions arise that account for the interaction between the inviscid and viscous regions. These additional terms and boundary conditions are necessary to calculate certain flows, such as thick boundary layers with an external rotational flow.[6,7]

The application of coupled methods has been the subject of many previous studies, mainly for subsonic and transonic flows.[8,9] Early investigations that examined the influence of second-order effects on hypersonic boundary-layer flow demonstrated the necessity to account for the vorticity at the edge of the boundary layer. This was generally achieved by an ad hoc method associated with the concept of "streamline swallowing."[10-12] Although it has been shown that this method can be employed with success for certain geometries, more generality can be obtained by solving the Euler equations for the flow in the outer (inviscid) region. To date, however, coupled Euler/boundary-layer calculations of hypersonic flows have generally considered only nonreactive flows or flow in chemical equilibrium.[13-16] The present paper, which treats nonequilibrium chemically reacting flows, is based on previous work of the authors,[17] extending the domain of application by an improved procedure for the matching of the inner and outer solutions. In addition, the method described in the present paper solves both the boundary-layer equations and the Euler equations to $\mathcal{O}(Re^{-1/2})$. The present paper thus, to the authors' knowledge, is the first to report complete second-order Euler/boundary-layer computations involving a consistent nonequilibrium calculation for the viscous and inviscid regions.

Among the advantages of coupled methods is the possibility to solve for the different flow regions using methods that are well suited to the local governing equations. Coupled Euler/boundary-layer methods can therefore take advantage of the wide existing base of experience in solving the Euler and boundary-layer equations using efficient and robust numerical techniques. This is particularly important for the industrial application of this method as a design tool. Thus, in many circumstances, the coupled Euler/boundary-layer method is preferred to other computationally efficient methods, such as the VSL or PNS methods.

It should be borne in mind, however, that the boundary-layer method—as well as the VSL and PNS methods—is based on a space-marching procedure in the streamwise direction. Regions of flow separation cannot therefore be treated except by the use of special techniques. One of the principal motivations for the application of a coupled Euler/boundary-layer method to hypersonic flows is the determination of the heat

Received Jan. 14, 1992; revision received May 9, 1992; accepted for publication May 29, 1992.

*Graduate Research Assistant, Institut de Machines Hydrauliques et de Mécanique des Fluides, ME-Ecublens, CH-1015.

†Research Scientist, Institut de Machines Hydrauliques et de Mécanique des Fluides, ME-Ecublens, CH-1015.

fluxes on the surface of re-entry vehicles. Since the maximum heating generally occurs on the windward surface where a space-marching method can be applied, the limitation to attached flows is not overly severe.

Recently, it has been shown[18] that, given identical physical and chemical models, the coupled Euler/boundary-layer method and the thin-layer Navier-Stokes method can provide very comparable flow solutions. This comparative study has confirmed the assertion that the computation time required for the coupled Euler/boundary-layer method is significantly less than required for even the thin-layer Navier-Stokes method.

Physical Modeling

The air in the flow region is considered to be a mixture of five species (N_2, O_2, NO, N, and O), each species being assumed to behave as a perfect gas. The pressure and enthalpy of the mixture are then given by

$$p = \rho R T \sum_s \frac{Y_s}{M_s}, \qquad h = \sum_s Y_s\, h_s\,(T) \tag{1}$$

where Y_s is the mass fraction ($Y_s = \rho_s/\rho$), h_s the enthalpy, and M_s the molar mass of species s. The enthalpy of each of the constituent species is written as a polynomial function of temperature having the following form:

$$\frac{h_s}{R_s\, T} = a_{1,s} + \frac{a_{2,s}}{2}T + \frac{a_{3,s}}{3}T^2 + \frac{a_{4,s}}{4}T^3 + \frac{a_{5,s}}{5}T^4 + \frac{a_{6,s}}{T} \tag{2}$$

The coefficients $a_{1,s}$, obtained from the fitting of theoretical data valid for temperatures up to 25,000 K (Ref. 19) are listed in Table 1. In Eq. (2), $R_s = R/M_s$ is the gas constant for species s.

For the general system of m reversible chemical reactions,

$$\sum_s \nu^a_{s,k} A_s \underset{k_{f,k}}{\overset{k_{b,k}}{\leftrightarrow}} \sum_s \nu^b_{s,k} A_s, \qquad k = 1, \ldots, m$$

where A_s denotes the chemical symbol of species s, and $\nu_{s,k}$ denotes the stoichiometric coefficients for species s corresponding to the reaction k. The rate of chemical production or destruction of a species s is given by

$$\dot{\omega}_s = M_s \sum_{k=1}^{m} (\nu^b_{s,k} - \nu^a_{s,k})\, k_{f,k}\, \rho^{m_1} \prod_i \left(\frac{Y_i}{M_i}\right)^{\nu^a_{i,k}} \times \left[1 - \frac{1}{K_{c,k}}\, \rho^{m_2} \prod_i \left(\frac{Y_i}{M_i}\right)^{(\nu^b_{i,k} - \nu^a_{i,k})}\right] \tag{3}$$

where

$$m_1 = \sum_s \nu^a_{s,k}, \qquad m_2 = \sum_s (\nu^b_{s,k} - \nu^a_{s,k})$$

Here, the forward and backward reaction rate constants for reaction k are denoted by $k_{f,k}$ and $k_{b,k}$, respectively.

In the present study, a chemical reaction scheme consisting of 17 reactions was employed.[20] The forward reaction rates are calculated from a modified Arrhenius equation:

$$k_{f,k} = B_k\, T^{\alpha k}\, e^{-E_k/T} \tag{4}$$

The backward reaction rates are determined via the equilibrium constants $K_{c,k}$, which are obtained using a fourth-order polynomial fit of experimental spectroscopic data:

$$k_{b,k} = \frac{k_{f,k}}{K_{c,k}}$$

$$K_{c,k}(T) = \exp(A_1 + A_2 Z + A_3 Z^2 + A_4 Z^3 + A_5 Z^4) \tag{5}$$

where $Z = (10^4/T)$. The coefficients B_k, α_k, and E_k for the forward reaction rates and the coefficients A_i, $i = 1, \ldots, 5$, for the equilibrium constants are as given by Park.[20]

The transport coefficients for viscosity μ, thermal conductivity λ, and multicomponent diffusion are obtained using the model of Straub,[21] which is based on a simplification of the general Chapman-Enskog theory. This model assumes that the molar weights of all molecules are the same (M_M = 30 kg/kmole) and similarly for the molar weights of atoms (M_A = 15 kg/kmole). This assumption reduces the number of binary diffusion coefficients from 11 to 3 and thus simplifies the calculation of the 20 multicomponent diffusion coefficients. The viscosity of the gas mixture is related to the viscosities of the constituent species by the semiempirical relation of Wilke.[22] The thermal conductivity of the mixture consists of two parts: a translational part that is calculated as if all of the constituent species were monoatomic and a part that accounts for the internal degrees of freedom of molecules. The contribution to the thermal conductivity of the mixture resulting from chemical reactions[23] is not considered in the present study.

Basic Equations

Inner Region

Using a body-oriented coordinate system, with x denoting the tangential direction and y the normal direction, the boundary-layer equations correct to second order in $Re^{-1/2}$ can be written as follows[4]:

Species continuity equation:

$$\rho \frac{u}{H}\frac{\partial Y_s}{\partial x} + \rho\, v \frac{\partial Y_s}{\partial y} = \dot{\omega}_s - \frac{1}{R}\frac{\partial}{\partial y}(R\, \rho\, Y_s\, V_{y,s}) - \kappa\, \rho\, Y_s\, V_{y,s} \tag{6}$$

Global continuity equation:

$$\frac{\partial}{\partial x}(R\rho u) + \frac{\partial}{\partial y}(H\, R\, \rho\, v) = 0 \tag{7}$$

Table 1 Polynomial coefficients used to calculate the thermodynamic properties of the constituent species of air (for each species, the upper row corresponds to the temperature range 300–5,000 K and the lower row to the range 5,000–250,000 K)

Species	a_1	a_2	a_3	a_4	a_5	a_6	a_7
N_2	3.1537e+00	9.9452e−04	−2.4649e−07	2.0863e−11	−3.2876e−18	−9.8236e+02	4.8001e+00
	7.7777e+00	−1.1912e−03	1.2541e−07	−3.0949e−12	−2.1690e−20	−8.5376e+03	−2.7306e+01
O_2	3.2670e+00	1.1324e−03	−2.7934e−07	2.5253e−11	2.0093e−17	−1.0243e+03	5.7227e+00
	2.2893e+00	6.7967e−04	−2.3506e−08	1.1871e−13	−5.3044e−20	2.8033e+03	1.4166e+01
NO	3.2374e+00	1.0949e−03	−3.0406e−07	2.7880e−11	5.8089e−18	9.8555e+03	6.5913e+00
	5.7368e+00	−4.6021e−04	5.2982e−08	−1.2892e−12	−1.3044e−20	6.4811e+03	−1.0167e+01
N	2.4957e+00	2.3583e−05	−2.3125e−08	6.3101e−12	1.7852e−19	5.6165e+04	4.2146e+00
	1.3388e+00	4.2074e−04	−2.9324e−08	9.1878e−13	4.3496e−20	5.8083e+04	1.2384e+01
O	2.6428e+00	−1.7596e−04	6.0750e−08	−5.2372e−12	−5.0993e−18	2.9215e+04	4.3691e+00
	2.3584e+00	8.8833e−05	−9.4390e−09	4.5843e−13	1.7023e−20	2.9356e+04	6.1065e+00

x momentum equation:

$$\rho\left(\frac{u}{H}\frac{\partial u}{\partial x}+v\frac{\partial u}{\partial y}+\kappa u v\right)=-\frac{1}{H}\frac{\partial p}{\partial x}+\frac{1}{R}\frac{\partial}{\partial y}\left(R\mu\frac{\partial u}{\partial y}\right)+\kappa\left(\mu\frac{\partial u}{\partial y}-u\frac{\partial \mu}{\partial y}\right) \tag{8}$$

y momentum equation:

$$\rho\kappa u^2=\frac{\partial p}{\partial y} \tag{9}$$

Energy equation:

$$\rho\frac{u}{H}\frac{\partial}{\partial x}\left(h+\tfrac{1}{2}u^2\right)+\rho v\frac{\partial}{\partial y}\left(h+\tfrac{1}{2}u^2\right)=\frac{1}{R}\frac{\partial}{\partial y}\left[R\left(\mu u\frac{\partial u}{\partial y}-q_y\right)\right]-\kappa\left[u\frac{\partial}{\partial y}(\mu u)+q_y\right] \tag{10}$$

In the previous equations,

$$H=1+\kappa(x)\,y \qquad R=[r(x)+y\cos\theta(x)]^m$$

where $\kappa(x)$ is the inverse longitudinal surface radius of curvature, $r(x)$ the body radius, $\theta(x)$ the angle between the body surface and the freestream direction, and $m=0$ for planar flow and 1 for axisymmetric flow. Equations (6–10) are valid if the local inverse radius of curvature is of order less than or equal to $Re^{-1/2}$; that is, $\mathcal{O}(1/\kappa)\leq\mathcal{O}(\delta)$, where δ is the boundary-layer thickness. Thus, these equations can be applied to flows of interest for which the boundary-layer concept is valid and exclude the case of "curvature dominated" flow.[16] The energy flux in the normal direction is the sum of the conductive and diffusive heat fluxes; that is,

$$q_y=-\lambda\frac{\partial T}{\partial y}+\rho\sum_s Y_s h_s V_{y,s} \tag{11}$$

where $V_{y,s}$ is the diffusion velocity in the normal direction for species s.

It can be noted that, if the longitudinal curvature effects are of $\mathcal{O}(Re^{-1/2})$, the previous equations to $\mathcal{O}(1)$ reduce to the classical Prandtl boundary-layer equations. The additional terms that arise in the second-order boundary-layer equations may be assigned physical interpretations that can be divided into the following three categories[7]: surface curvature effects (longitudinal and transverse), interaction with external flow (external vorticity and normal pressure gradients), and rarefied gas effects (velocity slip and temperature jump at the wall) that are not considered here.

In the present study, only three species equations are solved, the mass fractions of the other two species being determined from the resolution of the continuity equation for the mass fraction of elemental nitrogen, $Z_N=Y_N+Y_{N_2}+(M_N/M_{NO})Y_{NO}$:

$$\rho u\frac{\partial Z_N}{\partial x}+\rho v\frac{\partial Z_N}{\partial y}+\frac{1}{r^m}\frac{\partial}{\partial y}\left[r^m\rho\left(Y_N V_{y,N}+Y_{N_2}V_{y,N_2}+\frac{M_N}{M_{NO}}Y_{NO}V_{y,NO}\right)\right]=0 \tag{12}$$

and the conservation of species

$$\sum_s Y_s=1$$

The absence of a source term in Eq. (12) simplifies its numerical solution.

It is common to assume that Fick's law is valid for the high-temperature air mixture, with only binary diffusion being considered. If all species have the same Lewis number, it can be shown that the mass fraction of the elemental species is constant across the boundary layer.[19] In the present study, despite the simplification of the Straub model, multicomponent diffusion is, however, retained; thus variations of the mass fraction of the elemental species across the boundary layer are treated.

The boundary condition at the wall for the flow velocity is taken to be the usual no-slip condition ($u=v=0$). For the species continuity equations, two different wall conditions have been considered: a fully catalytic wall for which the chemical reactions at the wall are assumed to be catalyzed at a sufficiently high rate so that the mass fractions attain local equilibrium values and a noncatalytic wall for which no chemical reactions occur and hence there is no diffusion of any species at the wall. A fixed value for the wall temperature is imposed in the present study.

The pressure across the first-order boundary layer is given by the surface pressure determined from the Euler calculation. Given the stagnation point enthalpy, Eqs. (7) and (10), neglecting the normal gradients and second-order terms, can then be employed to calculate the enthalpy and tangential velocity along the entire boundary-layer edge. To determine the required mass fractions for a nonequilibrium boundary-layer flow, the classic paper of Fay and Riddell[24] assumes the flow at the edge of the boundary-layer stagnation line to be in local chemical equilibrium. For thick boundary layers, however, this assumption is generally not valid. In the present study, the species mass fractions at the edge of the boundary-layer stagnation line for the first-order calculation are therefore set to the surface values obtained at the stagnation point from the first-order Euler calculation. Equation (6), neglecting the normal gradients and second-order terms, can then be used to calculate the mass fractions along the edge of the boundary layer. Consistent with the neglect of diffusion in the outer inviscid region, the mass fraction of elemental nitrogen at the edge of the boundary layer is set equal to its freestream value $Z_{N,e}=Z_{N,\infty}=0.769$.

For the second-order calculation, the required values of pressure, enthalpy, tangential velocity, and species mass fractions at the viscous-inviscid interface are obtained by interpolation of the results of the Euler calculation.

Outer Region

The flow in the outer (inviscid) region is governed by the Euler equations that can be written in conservative form in an (X,Y) Cartesian coordinate system as follows[25]:

$$\frac{\partial}{\partial t}w+\frac{\partial}{\partial X}F(w)+\frac{\partial}{\partial Y}G(w)=S \tag{13}$$

where

$$w=\begin{bmatrix}\rho Y_s\\ \rho\\ \rho U\\ \rho V\\ \rho E\end{bmatrix},\qquad F(w)=\begin{bmatrix}\rho Y_s U\\ \rho U\\ \rho U^2+p\\ \rho UV\\ U(\rho E+p)\end{bmatrix}$$

$$G(w)=\begin{bmatrix}\rho Y_s V\\ \rho V\\ \rho UV\\ \rho V^2+\rho\\ V(\rho E+p)\end{bmatrix},\qquad S=\begin{bmatrix}\dot{\omega}_s\\ 0\\ 0\\ 0\\ 0\end{bmatrix} \tag{14}$$

In the previous equation, E is the total energy defined as $E=e+(U^2+V^2)/2$ where e is the internal energy. To first order in $Re^{-1/2}$, these equations reduce to the Euler equations with the familiar boundary condition of zero normal velocity

at the wall. It can be observed that, to second order, the equations have the same form as the classical Euler equations since no viscous terms appear, these being of third or higher order.[4] The matching principle between the inner and outer regions applied to the second-order equations gives rise to displacement effects associated with the influence of the boundary layer on the inviscid flow region. It has been shown[26] that displacement effects can be accounted for in the inviscid calculation through the concept of an "equivalent source" at the wall. This source can be written in the form of a normal component of velocity at the wall, which is related to the first-order mass flow at the wall by

$$V(0) = \frac{1}{r\rho_e}\frac{\partial}{\partial x}(r\,\rho_e\,u_e\,\delta_1) \tag{15}$$

where the subscript e denotes the edge of the boundary layer and δ_1 is the displacement thickness given by

$$\delta_1 = \int_0^{\delta}\left(1 - \frac{\rho u}{\rho_e\,u_e}\right)\mathrm{d}y$$

For nonequilibrium chemically reacting flows, only three partial differential equations for the mass fractions are resolved; the mass fractions of both elemental nitrogen and oxygen are constant throughout the inviscid region and equal to their freestream values.

Numerical Method

Inner Region

The second-order boundary-layer equations, Eqs. (6–10), are solved using a fully implicit, finite difference scheme. First-order spatial differences are used for the convective terms, whereas the diffusive terms are discretized by second-order differences. Since the second-order boundary-layer equations are parabolic in nature, they are solved using the same space-marching technique as generally employed to resolve the first-order boundary-layer equations. An uncoupled, iterative approach is employed using a primitive variable formulation, without the use of any similarity transformation. The global continuity and x momentum equations are first solved simultaneously, with the y momentum equation used to update the pressure. The species continuity equations are then solved simultaneously, followed by the energy equation. To account for coupling between equations, iterations are performed at each station along the flow direction until the desired level of convergence is obtained.

Being strongly dependent on the temperature and the species mass fractions, the source term in the species continuity equations can generally not be treated explicitly. It has therefore been suggested[27] to split the source term into two parts: the terms proportional to the mass fraction considered are then treated implicitly whereas the remaining terms act as explicit source terms. The drawback of this technique for an uncoupled approach is that convergence is only ensured for small changes of the mass fraction, and thus a fine computational mesh is generally required. Moreover, whereas the sum over all of the source terms is equal to zero, the sum over each of the implicit and explicit parts of the source terms are nonzero: this can lead to an accumulation of errors and associated negative values for the mass fractions. In the present study, the source terms are linearized in the iteration number N in the following manner:

$$\dot{\omega}_s^N = \dot{\omega}_s^{N-1} + \sum_r \frac{\partial \dot{\omega}_r^{N-1}}{\partial Y_r^{N-1}}\left(Y_r^N - Y_r^{N-1}\right) \tag{16}$$

with the term proportional to Y_s^N then treated implicitly. This procedure has been found not to require a fine mesh and provides an efficient and robust method over the entire hypersonic range.[19, 28] A similar procedure, based on a spatial linearization in the streamwise direction, has been employed with success for a fully coupled approach.[29]

The term in Eq. (6) related to species diffusion across the boundary layer is a second-order derivative in the normal coordinate. However, when expressed in terms of the diffusion velocity, the highest order derivative is of first order, the diffusion velocity being calculated from the previous global iteration cycle (as is necessary for the treatment of multicomponent diffusion). The order of the equation is therefore artificially reduced, leading to a difficulty in the imposition of all of the boundary conditions. One possible approach to overcome this difficulty is to express the diffusion velocities in terms of the mass fraction gradient by means of binary diffusion, through the application of Fick's law. However, since Fick's law is strictly only valid for binary mixtures, the appropriate diffusion coefficients for a multicomponent mixture are not well defined. To determine the diffusion coefficients, a constant Lewis number (independent of species) throughout the flow is often assumed. These approximations, although not rigorously justified, have nevertheless been shown[30] in some cases to provide a good evaluation of the boundary-layer properties. A second approach, adopted in the present study, involves recovering a second-order derivative in the species continuity equation by adding to both sides a term proportional to the second derivative of the species mass fraction.[19] The influence of this term vanishes for the required converged solution. The continuity equation for elemental nitrogen, Eq. (12), is resolved in the same manner.

To initiate the space-marching procedure, an initial profile is required. For flow over a blunt body, the x momentum equation in the form of Eq. (8) cannot be applied to the stagnation line, since the tangential velocity is zero, $u(0,y) = 0$. A possible solution to this problem is to calculate a similarity solution at a close distance from the stagnation line. This technique has been widely used in the past[31] but is not very efficient because of the necessary transformation of the coordinate system. In the present study, the tangential velocity along the stagnation line has been normalized to its edge value: $u(x,y) = u_e(x)U(x,y)$, where $u_e(0) = 0$. Application of the symmetric condition at the stagnation line then allows the boundary-layer solution to be obtained in terms of $U(x,y)$.

Outer Region

The Euler equations are discretized using a space-centered finite volume scheme. Both second- and fourth-order artificial dissipation terms are added to avoid spurious oscillations in the vicinity of discontinuities and to suppress odd/even oscillations. The external bow shock is determined using a shock-fitting procedure, with internal shocks being captured by the numerical scheme. The time integration of the discretized Euler equations is carried out using an explicit fourth-order Runge-Kutta scheme.[25] The flow at the outflow boundaries is assumed to be supersonic, with an extrapolation providing the necessary conditions.

It has been shown[25] that no special procedures are required to treat the chemical source terms in the species continuity equations. The time step used in the Runge-Kutta time integration procedure is the minimum of the chemical and fluid dynamical time steps. The chemical time step is defined as

$$\Delta t_{\text{chem}} = \min_{1\le s\le 5}\left[\frac{\partial \dot{\omega}_s}{\partial(\rho Y_s)}\right]^{-1} \tag{17}$$

whereas the fluid dynamical time step is the minimum time step for all cells:

$$\Delta t_{\text{fluid}} = \min_{\text{all }(i,j)}\left(\frac{\Delta t_{i,j}^I\,\Delta t_{i,j}^J}{\Delta t_{i,j}^I + \Delta_{ti,j}^J}\right) \tag{18}$$

where

$$\Delta t_{i,j}^I = \frac{S_{i,j}}{\lambda_{i,j}^I}, \qquad \Delta t_{i,j}^J = \frac{S_{i,j}}{\lambda_{i,j}^J}$$

where $S_{i,j}$ is the area of cell (i, j), and $\lambda^I_{i,j}$ and $\lambda^J_{i,j}$ are the spectral radii in the I and J directions, respectively.

For the shock-fitting procedure, the chemical composition is considered to be frozen across the shock wave. Since the shock wave is assumed to be infinitesimally thin (in reality, only a few mean free path lengths), there is insufficient time in traversing the shock for chemical reactions to take place; the composition of the air downstream of the shock wave is thus the same as that upstream. The variables behind the shock wave can therefore be calculated in a similar manner to the shock-fitting procedure employed for a nonreacting flow.

At the wall, the only physical boundary condition to impose is the value of the normal component of velocity. For the first-order calculation, this value is zero, and hence so are all the normal fluxes. It is thus only necessary to evaluate the contribution of the pressure to the convective flux. For the second-order calculation, however, the normal component of velocity at the wall is given by Eq. (15). The normal fluxes at the wall are therefore nonzero, and the physical quantities have to be evaluated at the wall. For both the first-order and second-order calculations, the required values of the physical quantities at the wall are obtained by linear extrapolation from the computational domain.

Coupling Procedure

The coupling method is a four-step procedure that successively resolves a set of equations of increasing order in $Re^{-1/2}$. The first-order Euler equations are first solved for the flow quantities in the outer inviscid region. The calculated surface pressure and the stagnation point values of mass fractions are then used to resolve the first-order boundary-layer equations. From the results of the latter calculation, the location of the viscous-inviscid interface is determined, as well as the equivalent source terms at the wall required for the second-order Euler calculation. Following the second-order Euler calculation, a computational mesh for the new inner region (defined as region between the wall and the viscous-inviscid interface) is then constructed to perform the second-order boundary-layer calculation. As mentioned earlier, the required boundary values at the interface are obtained from the second-order Euler calculation by interpolation.

It should be noted that the present method is consistent, to second order in $Re^{-1/2}$, with the asymptotic matching theory of Van Dyke.[3] However, rather than expressing the values of the required flow quantities at the viscous-inviscid interface in terms of a Taylor expansion of the inviscid flow values at the wall,[17] the interpolated values at the edge of the boundary layer are used. This procedure yields a good matching of the inner and outer solutions even if the inviscid flow solution has, for example, variable vorticity throughout the boundary-layer region.[16]

The choice of the location of the viscous-inviscid interface for the second-order boundary-layer calculation is somewhat arbitrary, since the definition of the boundary-layer edge is not unique. It is usual to define the boundary-layer thickness $\delta_{u,99}$ as the distance at which the tangential velocity u of the first-order boundary-layer solution equals 99% of its limiting value u_e. A study has been undertaken to determine the influence of this parameter on the computed boundary-layer flow. We define the quantity $\Delta C_f(\sigma, X)$ as the percentage change of the skin friction coefficient C_f [defined by Eq. (19)] at the location X, calculated with the viscous-inviscid interface at a distance $\delta_{u,\sigma}$ from the wall, relative to the value of C_f calculated with the interface at $\delta_{u,99}$.

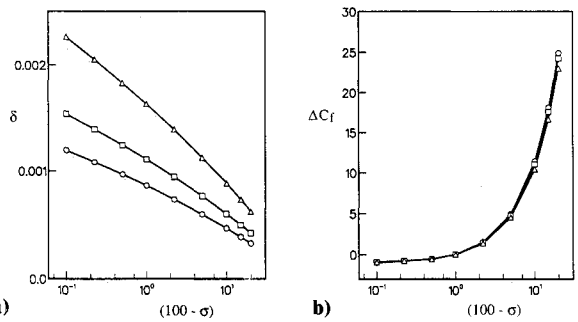

Fig. 1 Plots of a) boundary layer thickness $\delta_{u,\sigma}$ and b) percentage change of the skin friction coefficient ΔC_f for three angles (30 deg: ○, 45 deg: □, and 60 deg: △) as a function of $100 - \sigma$, where σ varies from 80 to 99.9.

As an example of the influence of the interface location on the computed boundary-layer flow, we present here results obtained for flow over a sphere at $M_\infty = 12.7$ with the freestream conditions listed in the following section. Figure 1 shows the calculated values of $\delta_{u,\sigma}$ and $\Delta C_f(\sigma, X)$ for three different angular positions as a function of the parameter $(100 - \sigma)$ where σ varies from 80 to 99.9. From Fig. 1b it can be observed that a choice of the interface location too close to the wall (e.g., $\sigma < 98$) leads to large increase in the calculated skin friction coefficient. Although not shown in Fig. 1b, an interface location chosen to be too distant from the wall also leads to large errors in C_f. Between these two extremes a "plateau" region can be observed for which the calculated values of C_f are essentially independent of σ. A study of different flow cases has revealed that the extent of this plateau region depends on the thickness of the boundary layer relative to the shock layer. For the flow conditions considered here, the boundary layer is relatively thin, and hence the plateau region is large. For thick boundary layers (as are present for high Mach number, high-altitude re-entry flows), the plateau region, although being much narrower, has been found to have roughly the same upper (in terms of $100 - \sigma$) border. An optimum position of the viscous-inviscid interface, which can be generally applied to different flow cases, is then the smallest distance from the wall that produces a calculated boundary-layer flow that is essentially independent of σ. For this reason, a value of $\delta_{u,99}$ has therefore been chosen for the location of the interface.

In the present study, the tangential velocity u has been used to determine the boundary-layer thickness. However, different boundary-layer thicknesses can be defined with reference to the normal profiles of other first-order boundary-layer quantities. An investigation has revealed that the temperature and total enthalpy profiles (with an appropriate choice of σ) can also be employed to provide a suitable location of the viscous-inviscid interface.

It has been observed[32] that, for flows in chemical nonequilibrium, the results of Euler calculations are inherently inaccurate in a narrow "chemical layer" in the close vicinity of the wall. For the coupled method described in the present paper, it is therefore important to note that the second-order boundary-layer calculations require only the values of the inviscid quantities at the interface. Since the chemical layer has been shown to be of much smaller extent than the boundary layer, this inaccuracy is not reflected in the computed boundary-layer results.

The matching procedure employed in the coupling method described in this paper enforces continuity of the pressure, enthalpy, tangential velocity, and species mass fractions (and hence density and temperature) at the viscous-inviscid interface. However, since there is no matching condition required for the normal component of velocity, continuity of the local Mach number is not guaranteed. In addition, continuity of the derivatives of the flow quantities across the interface is not ensured. The extent to which all of the flow quantities and their derivatives are continuous across the interface (as is physically required) is a measure of the validity of the neglect of higher order terms in the expansion of the governing equations.

Finally, the previously described coupling method requires both first-order and second-order boundary-layer and Euler calculations to be performed in a consecutive manner. Thus, a

larger computation time is required than for a first-order calculation alone. It should be noted, however, that the second-order Euler calculation is initiated using the first-order result, leading to a computation time for both Euler calculations that is less than twice the time used for only the first-order calculation. In addition, each of the boundary-layer calculations requires significantly less computation time than an Euler calculation to obtain a comparable degree of accuracy.

Numerical Examples

The coupled Euler/boundary-layer method described in the previous sections has been applied to a number of different flow cases of interest. To illustrate this application, nonequilibrium hypersonic flows over both a double ellipse and a sphere are considered in some detail in the following sections.

For all of the test cases presented here, a series of computations has been performed using different size meshes to ascertain that a mesh-independent solution has been obtained. The results are presented for the finest meshes considered; essentially identical results have been obtained using coarser meshes with half the number of mesh points.

Flow over a Double Ellipse

The double ellipse geometry, which has been considered for a series of test cases at the recent Workshop in Hypersonic Flows for Reentry Problems, is defined as follows[33]:

$$\left(\frac{X}{0.60}\right)^2 + \left(\frac{Y}{0.15}\right)^2 = 1 \qquad X \le 0,$$

$$\left(\frac{X}{0.35}\right)^2 + \left(\frac{Y}{0.25}\right)^2 = 1 \qquad X \le 0,\ Y \ge 0$$

The double ellipse section is extended by a flat plate of length 0.16 m. Calculations have been undertaken for flow at an angle of attack of 30 deg, with the following conditions: $M_\infty = 25$, $Re_\infty = 2.2 \times 10^4\ \mathrm{m}^{-1}$, $T_\infty = 56$ K, and $T_w = 1500$ K.

The freestream conditions for this flow case have been chosen so that strong nonequilibrium chemical effects take place with a high level of molecular dissociation. Since the Reynolds number is relatively low, the boundary layer is thick, and second-order effects can be expected to play an important role in determining the flow characteristics. Nonequidistant meshes of 180×50 points for the Euler calculations and 200×100 points for the boundary-layer calculations were used.

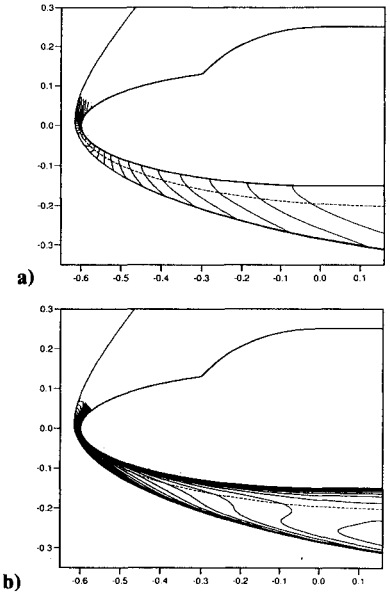

Fig. 2 Contour plots of a) pressure coefficient and b) temperature for flow over the double ellipse. Line spacing: $\Delta C_p = 0.1$; $\Delta T = 500$ K. Viscous-inviscid interface, ------.

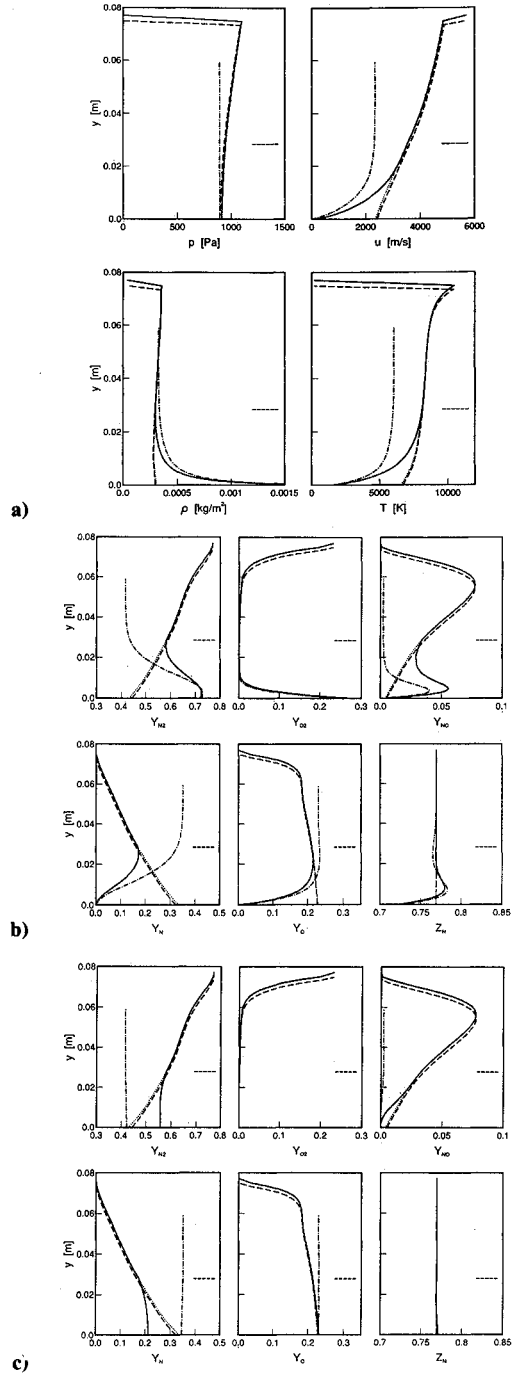

Fig. 3 Normal profiles for flow over the double ellipse of a) pressure, tangential velocity, density, and temperature; and b) and c) species mass fractions. Plots a and b are for a fully catalytic wall and plot c is for a noncatalytic wall. Second-order coupled solution, ——; first-order inner region, -·-·-; outer region: first-order, — — —; second-order, ·····. The location of the viscous-inviscid interface is indicated by ------.

Contour plots of the pressure coefficient and temperature calculated throughout the flow region using the coupled Euler/boundary-layer method are shown in Fig. 2. For this flow case, the viscous region occupies about 40% of the shock layer. Since the present method cannot be applied to regions of strong viscous-inviscid interaction, the boundary-layer calculations have not been undertaken on the upper surface of the body. It should also be noted that, although the angle of attack is 30 deg, the position of the stagnation point deter-

mined by the Euler calculation is at the angle of about 35 deg. This effect, due to the curvature of the stagnation line, leads to only a slight inaccuracy in the initial solution of the second-order boundary-layer calculation (which assumes a straight stagnation line).

The results of both first-order and second-order calculations are presented in Fig. 3, which shows profiles of the flow quantities calculated for a streamwise station midway along the ellipse section at $X = -0.3$ m. Although the results shown in Fig. 3a were obtained assuming a fully catalytic wall, very similar profiles were calculated for a noncatalytic wall. On the contrary, a comparison of the profiles of the species mass fractions shown in Fig. 3b (for a fully catalytic wall) and Fig. 3c (for a noncatalytic wall) reveals large differences.

Figure 3a clearly shows that the inclusion of second-order terms has a strong influence on the boundary-layer calculation. In particular, although the pressure employed for the first-order calculation is constant across the boundary layer, normal pressure gradients are observed in the second-order profile arising from the longitudinal surface curvature.[15,17] Similarly, to first order the flow at the edge of the boundary layer is irrotational, whereas second-order effects are shown to account for the presence of vorticity at the interface. The influence of second-order effects on the inviscid flow is seen to be much less significant. Accounting for displacement effects, however, is shown to lead to an increase of about 4% in the shock-layer thickness.

Substantial differences in the profiles of the species mass fractions can be observed as the result of the inclusion of second-order effects. Figure 3b shows that a fully catalytic wall with the chosen wall temperature produces a recombination of molecular nitrogen and oxygen across the boundary layer; the recombination in the vicinity of the interface is, however, significantly higher for the second-order calculation. The first-order results obtained for a noncatalytic wall (Fig. 3c) shows that the gradients in the species mass fractions across the boundary layer are negligibly small. However, second-order effects are seen to lead to mass fraction gradients, as well as an enhanced recombination in the boundary-layer region. These changes are associated with the observed increase in the calculated temperature of the boundary layer as a result of the influence of second-order effects.

Figure 3 clearly demonstrates that, with the inclusion of second-order effects, an excellent matching of the inner and outer solutions can be obtained. It can be observed that,

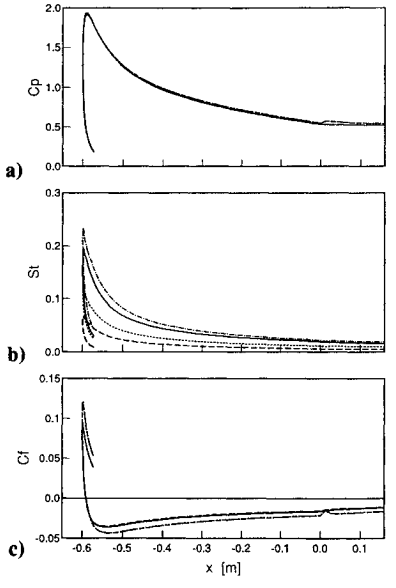

Fig. 4 Values of a) pressure coefficient, b) Stanton number, and c) skin friction coefficient calculated along the surface of the double ellipse. Fully catalytic wall: first-order ——, second-order, ·····; noncatalytic wall: first-order, — — —, second-order, -----.

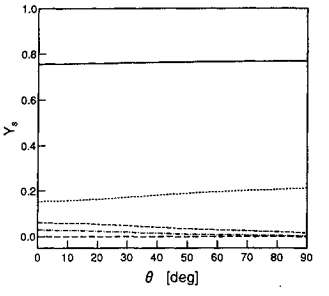

Fig. 5 Mass fractions calculated at the viscous-inviscid interface for flow over the sphere for species: N_2,——; O_2,-----; NO, ·····; N, — — —; and O, —·—.

despite the thickness of the boundary layer, not only the thermodynamical and chemical quantities are continuous across the interface (as imposed) but also are—to a surprisingly large degree—their derivatives. As mentioned in the previous section, this provides a measure of confidence in the accuracy of the method.

Figure 4 shows plots of the surface pressure coefficient C_p, Stanton number St, and skin friction coefficient C_f defined as follows:

$$C_p = \frac{p - p_\infty}{\tfrac{1}{2}\rho_\infty u_\infty^2}$$

$$St = \frac{q_{y,w}}{\rho_\infty u_\infty c_{p\infty}(T_{0\infty} - T_w)}$$

$$C_f = \frac{\mu_w \left[\dfrac{\partial u}{\partial y}\right]_w}{\tfrac{1}{2}\rho_\infty u_\infty^2} \tag{19}$$

where $T_{0\infty}$ is the total enthalpy divided by the freestream specific heat. Figure 4 shows the surface coefficients calculated from both first-order and second-order theories for both fully catalytic and noncatalytic wall conditions.

Since the pressure gradients across the shock layer are small (as shown in Fig. 3a) and insensitive to the wall catalyticity, only a slight difference is observed between the surface pressure coefficients shown in Fig. 4. The inclusion of second-order effects, however, results in a large increase in both the Stanton number and the skin friction coefficient, for both fully catalytic and noncatalytic wall surfaces. These increases are associated with the strong modification of both the temperature and tangential velocity profiles in the boundary-layer region, as observed in Fig. 3a. At the maximum value of skin friction, there is an increase of 25% between the first-order and second-order calculations. For the Stanton number, the influence of second-order effects is greater for a noncatalytic wall than for a fully catalytic wall. This is because, for a fully catalytic wall having a fixed temperature, almost identical wall values of mass fraction are obtained from the first-order and second-order calculations. (Note that the sharp feature observed near $X = 0$, particularly in the C_p and C_f values, is caused by the discontinuity of the surface radius of curvature at this location.)

Flow over a Sphere

For this flow case, a sphere of 50 mm radius has been considered with the following conditions: $M_\infty = 12.7$, $Re_\infty = 4.3 \times 10^5\ \mathrm{m}^{-1}$, $T_\infty = 196$ K, and $T_w = 300$ K. These conditions have been chosen to allow a comparison with the experimental shock tunnel results reported by Olivier et al.[34] The freestream enthalpy for this flow case is much lower than that of the previous case; hence the level of molecular dissociation in the flow region is expected to be much lower. In addition, as a result of the higher Reynolds number, second-order effects

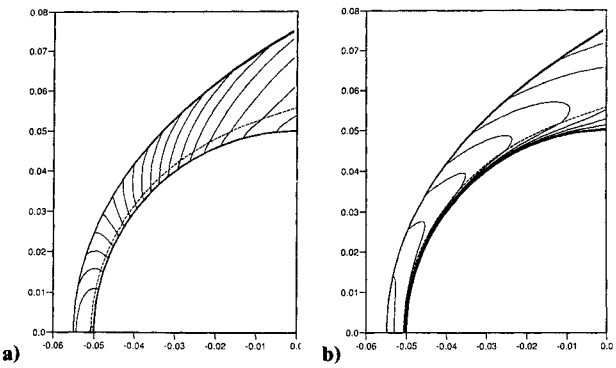

Fig. 6 Contour plots of a) pressure coefficient and b) temperature for flow over the sphere. Line spacing: $\Delta C_p = 0.1$; $\Delta T = 500$ K. Viscous-inviscid interface, ------.

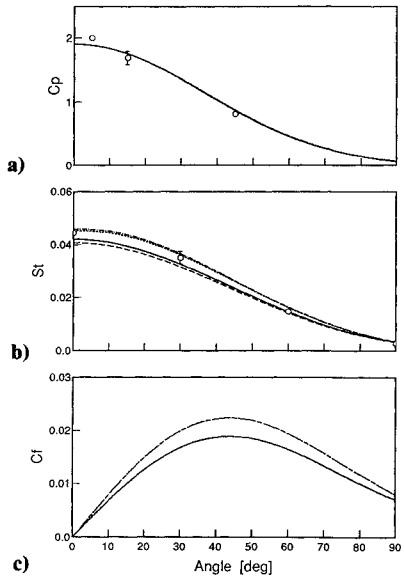

Fig. 7 Values of a) pressure coefficient, b) Stanton number, and c) skin friction coefficient calculated along the surface of the sphere. Fully catalytic wall: first-order, ——, second-order, ·····; noncatalytic wall: first-order, — — —, second-order, ------. The open circles indicate the experimentally measured values of C_p and St.[34]

should also be more modest. Nonequidistant meshes of 100×50 points for the Euler calculations and 200×100 points for the boundary-layer calculations were used for this flow case.

To gauge the extent of dissociation for this flow case, Fig. 5 shows the mass fractions of each species calculated at the viscous-inviscid interface. This plot indeed shows that, for the flow conditions considered, there is a modest dissociation of N_2 and O_2 into NO and O. However, the temperature of the flow is not sufficiently elevated to cause a noticeable production of atomic nitrogen.

Contour plots of the pressure coefficient and temperature in the flow region around the windward surface of the sphere, calculated using the coupled Euler/boundary-layer method, are given in Fig. 6. These plots indicate that the viscous region occupies only about 15% of the shock-layer region.

Figure 7 shows the calculated values of the surface coefficients, for both fully catalytic and noncatalytic wall surfaces. A maximum increase of 20% is found for the skin friction coefficient between first-order and second-order calculations, whereas the increase in Stanton number is about 10%. Only slight differences are observed between the results obtained for fully catalytic and noncatalytic wall surfaces, due to the low level of dissociation. Also shown in Fig. 7 is the experimentally measured values of C_p and St, the surface of the sphere being considered to be essentially fully catalytic. From this figure, it can be observed that accurate determinations of both the pressure coefficient and Stanton number are obtained using the present coupled method.

Conclusions

A coupled Euler/boundary-layer method to calculate hypersonic flows in chemical nonequilibrium has been presented. This method utilizes the robust computational techniques developed in the past for both the resolution of the Euler equations for the inviscid flow region and the boundary-layer equations for the viscous region. It has been shown that the introduction of terms of second order in $Re^{-1/2}$ does not change the basic mathematical nature of these sets of equations. Suitable techniques for the determination of the viscous-inviscid interface and the matching conditions to be applied along this interface have been elaborated.

For an example of a flow case having a low Reynolds number (and consequently a thick boundary layer) and high freestream enthalpy (and thus strong nonequilibrium chemistry effects), a strong influence due to second-order effects has been observed. It has been shown that second-order effects play a major role in determining the wall coefficients of skin friction and Stanton number. Moreover, the inclusion of second-order terms has been shown to enable a good matching of the calculated profiles at the viscous-inviscid interface for both chemical and thermodynamical properties. The results of the calculations presented clearly demonstrate that under these circumstances a first-order boundary-layer calculation is not able to determine the flow quantities with sufficient accuracy. However, even for the somewhat extreme conditions considered, the coupled Euler/boundary-layer method employed is able to provide a much more physical flow solution.

The surface coefficients calculated for a flow exhibiting more modest second-order and chemical effects has shown excellent agreement with available experimental results. Together with the results of a comparison of the present method with a thin-layer Navier-Stokes method,[18] this indicates that the coupled Euler/boundary-layer method can provide an accurate and efficient calculation of nonequilibrium, chemically reacting hypersonic flows.

Acknowledgments

This work was performed under contract from Dassault Aviation within the framework of the Hermes Aerodynamics R&D Program. Financial support was also provided by the Commission Suisse pour l'Encouragement de la Recherche Scientifique. The authors would like to thank I. L. Ryhming for his interest and encouragement throughout the present study and J. B. Vos for providing the first-order Euler code.

References

[1]Bertin, J. J., Glowinski, R., and Periaux, J. (eds.), *Hypersonics, Vol. I—Defining the Hypersonic Environment*, Vol. 8, Progress in Scientific Computing, Birkhäuser, Boston, MA, 1989.

[2]Greenberg, J. B., "Operator Splitting Methods for the Computation of Reacting Flows," *Computers and Fluids*, Vol. 11, No. 2, 1983, pp. 95-105.

[3]Van Dyke, M., *Perturbation Methods in Fluid Mechanics*, Academic Press, New York, 1964.

[4]Grundmann, R., "Boundary Layer Equations and Methods of Solution," *Computational Fluid Dynmamics: An Introduction*, edited by J. F. Wendt, Springer-Verlag, Berlin, Germany, 1992, Chap. 8, pp. 151-179.

[5]Lagerstrom, P. A., "Note on the Preceding Two Papers," *Journal of Mathematics and Mechanics*, Vol. 6, 1957, pp. 605, 606.

[6]Van Dyke, M., "Higher Approximations in Boundary-Layer Theory: Part 1—General Analysis," *Journal of Fluid Mechanics*, Vol. 14, 1962, Pt. 2, pp. 161-177.

[7]Van Dyke, M., "Higher-Order Boundary Layer Theory," *Annual Review of Fluid Mechanics*, Vol. 1, 1969, pp. 265-292.

[8]Lock, R. C., and Williams, B. R., "Viscous-Inviscid Interactions in External Aerodynamics," *Progress in Aerospace Sciences*, Vol. 24, No. 2, 1987, pp. 51-171.

[9]Monnoyer de Galland, F., "Calculation of Three-Dimensional Attached Viscous Flow on General Configurations Using Second-Order Boundary-Layer Theory," *Zeitschrift für Flugwissenschaften und Weltraumforschung*, Vol. 14, 1990, pp. 95–108.

[10]Levine, J. N., "Finite Difference Solution of the Laminar Boundary Layer Equations Including Second-Order Effects," AIAA Paper 68-739, June 1968.

[11]Mayne, A. W., and Adams, J. C., "Streamline Swallowing by Laminar Boundary Layers in Hypersonic Flows," Arnold Engineering Development Center, AEDC-TR-71-32, Arnold Air Force Station, TN, March 1971.

[12]DeJarnette, F. R., and Hamilton, H. H., "Aerodynamic Heating on 3-D Bodies Including the Effects of Entropy-Layer Swallowing," AIAA Paper 74-602, June 1974.

[13]Davis, R. T., and Flügge-Lotz, I., "Second-Order Boundary-Layer Effects in Hypersonic Flow Past Axisymmetric Blunt Bodies," *Journal of Fluid Mechanics*, Vol. 20, Part 4, 1964, pp. 593–623.

[14]Mundt, C., Pfitzner, M., and Schmatz, M. A., "Calculation of Viscous Hypersonic Flow Over Flared Cones," *Proceedings of the Eighth GAMM Conference on Numerical Methods in Fluid Mechanics*, edited by P. Wesseling, Vol. 29, Vieweg, Braunschweig, Germany, 1990, pp. 419–429.

[15]Monnoyer, F., Mundt, C., and Pfitzner, M., "Calculation of Hypersonic Viscous Flow Past Reentry Vehicles with an Euler-Boundary Layer Coupling Method," AIAA Paper 90-0417, Jan. 1990.

[16]Aupoix, B., Brazier, J. Ph., Cousteix, J., and Monnoyer, F., "Second-Order Effects in Hypersonic Boundary Layers," *Proceedings of the Third Joint Europe/U.S. Short Course in Hypersonics* (Aachen, Germany), Oct. 1990; see also Aupoix, B., Brazier, J. Ph., and Cousteix, J., "Asymptotic Defect Boundary-Layer Theory Applied to Hypersonic Flows," *AIAA Journal*, Vol. 30, No. 5, 1992, pp. 1252–1259.

[17]Sawley, M. L., and Wüthrich, S., "Non-Equilibrium Hypersonic Flow Simulations Using the Second-Order Boundary Layer Equations," *Computational Methods in Applied Mechanics and Engineering*, Vol. 89, 1991, pp. 129–140.

[18]Wüthrich, S., Perrel, F., Sawley, M. L., and Lafon, A., "Comparison of Thin Layer Navier-Stokes and Coupled Euler/Boundary Layer Calculations of Non-Equilibrium Hypersonic Flows," *Proceedings of the Ninth GAMM Conference on Numerical Methods in Fluid Mechanics*, edited by J. B. Vos, A. Rizzi, and I. L. Ryhming, Vol. 35, Notes on Numerical Fluid Mechanics, Vieweg, Braunschweig, Germany, 1992, pp. 138–147; see also Inst. de Machines Hydrauliques et de Mécanique des Fluides Rept. T-92-3, Lausanne, Switzerland, March 1992 (submitted for publication in *Computers and Fluids*).

[19]Sawley, M. L., and Wüthrich, S., "The Computation of Chemically-Reacting and Radiating Hypersonic Boundary Layer Flows," Inst. de Machines Hydrauliques et de Mécanique des Fluides, Rept. T-91-20, Lausanne, Switzerland, Oct. 1991.

[20]Park, C., "On Convergence of Computation of Chemically Reacting Flows," AIAA Paper 85-0247, Jan. 1985.

[21]Straub, D., "Exakte Gleichungen für die Transportkoeffizienten eines Fünfkomponentengemisches als Modellgas Dissoziierter Luft," Deutsche Luft- und Raumfahrt, Freiburg im Breisqau, Germany, Rept. DLR-FB 72-34, May 1972.

[22]Wilke, C. R., "A Viscosity Equation for Gas Mixtures," *Journal of Chemical Physics*, Vol. 18, No. 4, 1950, pp. 517–519.

[23]Hirschfelder, J. O., Curtiss, C. F., and Bird, R. B., *Molecular Theory of Gases and Liquids*, 2nd ed., Wiley, New York, 1964, p. 1196.

[24]Fay, J. A., and Riddell, F. R., "Theory of Stagnation Point Heat Transfer in Dissociated Air," *Journal of the Aeronautical Sciences*, Vol. 25, No. 2, 1958, pp. 73–85.

[25]Vos, J. B., and Bergman, C. M., "Chemical Equilibrium and Non-Equilibrium Inviscid Flow Simulation Using an Explicit Scheme," *Computer Physics Communications*, Vol. 65, 1991, pp. 289–298.

[26]Lighthill, M. J., "On Displacement Thickness," *Journal of Fluid Mechanics*, Vol. 4, Pt. 4, 1958, pp. 383–392.

[27]Blottner, F. G., Johnson, M., and Ellis, M., "Chemically Reacting Viscous Flow Program for Multi-Component Gas Mixtures," Sandia Lab., SC-RR-70-754, Albuquerque, NM, 1971.

[28]Sawley, M. L., and Wüthrich, S., "Non-Equilibrium Hypersonic Flow Simulations Using a Coupled Euler/Boundary Layer Method," *Proceedings of the First European Symposium on Aerothermodynamics for Space Vehicles*, European Space Agency SP-318, Noordwijk, The Netherlands, May 1991, pp. 387–392.

[29]Blottner, F. G., "Nonequilibrium Laminar Boundary Layer Flow of Ionized Air," General Electric Co., R64SD56, King of Prussia, PA, Nov. 1964; see also *AIAA Journal*, Vol. 2, No. 11, 1964, pp. 1921–1927.

[30]Eldem, C., "Couches Limites Hypersoniques avec Effects de Dissociation," Doctoral Thesis, L'Ecole Nationale Supérieure de l'Aéronautique et de l'Espace, Toulouse, France, Dec. 1987.

[31]Cousteix, J., and Aupoix, B., "Calculations of Hypersonic Laminar Boundary Layers," *Hypersonics, Vol. II—Computation and Measurement of Hypersonic Flows*, edited by J. J. Bertin, R. Glowinski, and J. Periaux, Vol. 9, Progress in Scientific Computing, Birkhäuser, Boston, MA, 1989, pp. 93–149.

[32]Désidéri, J.-A, "Some Comments on the Numerical Computations of Reacting Flows over the Double Ellipse (Double Ellipsoid), *Hypersonic Flows for Reentry Problems*," edited by J.-A. Désidéri, R. Glowinski, and J. Périaux, Vol. 2, Springer-Verlag, Berlin, Germany, 1991, pp. 871–881.

[33]Désidéri, J.-A., Glowinski, R., and Periaux, J. (eds.), *Hypersonic Flows for Reentry Problems*, Vol. 2, Springer-Verlag, Berlin, Germany 1991, pp. 17–24.

[34]Olivier, H., Vetter, M., and Grönig, H., "High Enthalpy Testing in the Aachen Shock Tunnel TH 2," *Proceedings of the First European Symposium on Aerothermodynamics for Space Vehicles*, European Space Agency SP-318, Noordwijk, The Netherlands, May 1991, pp. 377–384.